BULLETIN OF THE POLISH ACADEMY OF SCIENCES
TECHNICAL SCIENCES, Vol. 63, No. 3, 2015
DOI: 10.1515/bpasts-2015-0089

Recent developments in simulation-driven multi-objective design of antennas

S. KOZIEL[1]* and A. BEKASIEWICZ[2]

[1] Engineering Optimization & Modeling Center, School of Science and Engineering, Reykjavík University, Menntavegur 1, 101 Reykjavík, Iceland
[2] Faculty of Electronics, Telecommunications and Informatics, Gdansk University of Technology, 11/12 Narutowicza St., 80-233 Gdansk, Poland

Abstract. This paper addresses computationally feasible multi-objective optimization of antenna structures. We review two recent techniques that utilize the multi-objective evolutionary algorithm (MOEA) working with fast antenna replacement models (surrogates) constructed as Kriging interpolation of coarse-discretization electromagnetic (EM) simulation data. The initial set of Pareto-optimal designs is subsequently refined to elevate it to the high-fidelity EM simulation accuracy. In the first method, this is realized point-by-point through appropriate response correction techniques. In the second method, sparsely sampled high-fidelity simulation data is blended into the surrogate model using Co-kriging. Both methods are illustrated using two design examples: an ultra-wideband (UWB) monocone antenna and a planar Yagi-Uda antenna. Advantages and disadvantages of the methods are also discussed.

Key words: computer-aided design (CAD), antenna design, multi-objective optimization, surrogate models, evolutionary algorithms.

1. Introduction

One of the most important steps in the design process of antenna structures is adjustment of their geometry and/or material parameters. The aim is to satisfy given performance specifications concerning antenna reflection, gain, radiation pattern, and, more and more often, physical dimension (size, footprint) [1–39]. For the sake of reliability, the adjustment process normally relies on high-fidelity electromagnetic (EM) simulation [1–3]. It is particularly important for contemporary structures for which theoretical models either are not available or are very inaccurate. Also, in many cases it is necessary to account for EM interactions between the antenna itself and its environment (connectors, housing, installation fixtures, etc.).

Perhaps the most common approach to geometry adjustment is parameter sweeps guided by engineering insight. Unfortunately, this method is laborious and does not guarantee optimum results, especially when the number of independent parameters is large. Automated geometry optimization is therefore highly desirable, however, quite challenging [37–39]. Majority of conventional techniques (such as gradient-based algorithms or derivative free methods, e.g., pattern search algorithms) require considerable number of objective function evaluations (and, associated EM simulations) to yield an optimized design [4]. Recent availability of adjoint sensitivity techniques [5, 6] through certain commercial simulation software packages (e.g., [7, 8]) revived interest in gradient optimization. On the other hand, surrogate-based optimization (SBO) techniques [9–13] allow for dramatic reduction of the design optimization costs by shifting most of the operations into cheap replacement models (surrogates). The latter, in case of antennas, are normally constructed using coarse-discretization EM simulations [14].

For the sake of simplicity, most of antenna optimization problems are reformulated as single objective ones, where one primary objective is handled directly, whereas the others are controlled through appropriately defined constraints or penalty functions ([15]). However, real-world antenna design tasks are multi-objective ones. In particular, if the designer priorities are not clearly defined beforehand, identifying a set of alternative design representing the best possible trade-offs between conflicting objectives may be of fundamental importance (e.g., in order to determine limitations of a given antenna structure and its suitability for a given application) [16–19]. Nowadays, population-based metaheuristics are undoubtedly the most popular solution approaches for handling multi-objective antenna design problems. Techniques such as multi-objective genetic algorithms (GAs) and particle swarm optimizers (PSO), e.g., [16, 18–23], allow finding the entire Pareto front in one algorithm run. However, their disadvantage is high computational cost (hundreds, thousands or even tens of thousands of objective function evaluations), which becomes a serious bottleneck if high-fidelity discrete EM simulations are involved in antenna evaluation process.

Recently, two computationally efficient techniques for multi-objective design optimization of antennas have been proposed [24, 25]. Both methods rely on fast response surface approximation (RSA) surrogates created from sampled coarse-discretization EM simulation data, as well as refinement procedures intended to obtain representations of the Pareto-optimal sets at the high-fidelity EM antenna model level. The refinement strategy adopted in [24] is point-by-point

*e-mail: koziel@ru.is

identification using designs sampled from the initial Pareto set (obtained by optimizing the RSA) model, and suitable response correction techniques. In [25] refinement is realized by blending sparsely sampled high-fidelity EM model data into the RSA surrogate using Co-kriging [26]. In this paper, we review both methods, provide their unified formulation, illustrate and compare them using examples (an ultra-wideband monocone, and a planar Yagi-Uda antenna), as well as discuss their advantages and disadvantages.

2. Multi-objective antenna design using RSA models and variable-fidelity EM simulations

In this section, we formulate the multi-objective antenna design problem and introduce variable-fidelity EM models. We also describe Kriging and Co-kriging interpolation as fundamental tools for creating response surface approximation (RSA) surrogates utilized throughout the optimization process. Finally, we describe the optimization flow including two alternative options for Pareto set refinement.

2.1. Multi-objective antenna design. problem formulation. Let $\boldsymbol{R}_f(\boldsymbol{x})$ be a response (e.g., reflection or gain versus frequency) of an accurate model of the antenna structure under design. The response $\boldsymbol{R}_f(\boldsymbol{x})$ is obtained using high-fidelity EM simulation. Here, $\boldsymbol{x}$ is a vector of designable parameters, i.e., antenna dimensions.

We consider N_{obj} design objectives, $F_k(\boldsymbol{x})$, $k = 1, \ldots, N_{obj}$. A typical performance objective would be to minimize antenna reflection over a certain frequency band of interest, and to ensure that $|S_{11}| < -10$ dB over that band. There might be also geometrical objectives such as to minimize $F_k(\boldsymbol{x}) = A(\boldsymbol{x})$ – the antenna size defined in a convenient way (e.g., maximal lateral size, height, the maximal dimension, area of the footprint, antenna volume). Similar objectives can be formulated with respect to antenna gain, radiation pattern, efficiency, etc.

If $N_{obj} > 1$ then any two designs $\boldsymbol{x}^{(1)}$ and $\boldsymbol{x}^{(2)}$ for which $F_k(\boldsymbol{x}^{(1)}) < F_k(\boldsymbol{x}^{(2)})$ and $F_l(\boldsymbol{x}^{(2)}) < F_l(\boldsymbol{x}^{(1)})$ for at least one pair $k \neq l$, are not commensurable, i.e., none is better than the other in the multi-objective sense. We define Pareto dominance relation $\prec$ [27] saying that for the two designs $\boldsymbol{x}$ and $\boldsymbol{y}$, we have $\boldsymbol{x} \prec \boldsymbol{y}$($\boldsymbol{x}$ dominates $\boldsymbol{y}$) if $F_k(\boldsymbol{x}) < F_k(\boldsymbol{y})$ for all $k = 1, \ldots, N_{obj}$. The goal of the multi-objective optimization if to find a representation of a so-called Pareto front (of Pareto-optimal set) X_P of the design space X, such that for any $\boldsymbol{x} \in X_P$, there is no $\boldsymbol{y} \in X$ for which $\boldsymbol{y} \prec \boldsymbol{x}$ [27].

2.2. Variable-fidelity electromagnetic models. As mentioned in the introduction, the high-fidelity model $\boldsymbol{R}_f$ is computationally too expensive to be handled directly in multi-objective optimization. In this work, we speed up the design process by utilizing an auxiliary low-fidelity model $\boldsymbol{R}_c$, which is a coarse-discretization counterpart of $\boldsymbol{R}_f$. By appropriate mesh density manipulation and possible other simplifications (see, e.g., [28]), $\boldsymbol{R}_c$ can be made 20 to 50 times faster than $\boldsymbol{R}_f$, however, at the expense of some accuracy degradation. Because of this, as well as the fact that direct multi-objective optimization is usually too expensive even at the $\boldsymbol{R}_c$ level, our optimization methodology exploits response surface approximation models briefly described in the following Subsec. 2.3 and 2.4. The optimization algorithm is formulated in Subsec. 2.5.

2.3. Surrogate modeling. Kriging interpolation. Response surface approximation surrogates play a key role in the optimization methodology described in Subsec. 2.5. The first part of the process (identification of the initial Pareto set) is realized using a Kriging interpolation model constructed from sampled coarse-discretization model data. Kriging is a popular technique to interpolate deterministic noise-free data [29]. Let $X_{B.KR} = \{\boldsymbol{x}_{KR}^1, \boldsymbol{x}_{KR}^2, \ldots, \boldsymbol{x}_{KR}^{NKR}\} \subset X_R$ be the base (training) set and $\boldsymbol{R}_c(X_{B.KR})$ the associated low-fidelity model responses. The Kriging interpolant is derived as

$$\boldsymbol{R}_{s.KR}(\boldsymbol{x}) = M\alpha + r(\boldsymbol{x}) \cdot \Psi^{-1} \cdot (\boldsymbol{R}_f(X_{B.KR}) - F\alpha), \quad (1)$$

where M and F are Vandermonde matrices of the test point $\boldsymbol{x}$ and the base set $X_{B.KR}$, respectively. The coefficient vector α is determined by Generalized Least Squares (GLS). $r(\boldsymbol{x})$ is an $1 \times N_{KR}$ vector of correlations between the point $\boldsymbol{x}$ and the base set $X_{B.KR}$, where the entries are $r_i(\boldsymbol{x}) = \psi(\boldsymbol{x}, \boldsymbol{x}_{KR}^i)$, and Ψ is a $N_{KR} \times N_{KR}$ correlation matrix, with the entries given by $\Psi_{i,j} = \psi(\boldsymbol{x}_{KR}^i, \boldsymbol{x}_{KR}^j)$. In this work, the exponential correlation function is used, i.e., $\psi(\boldsymbol{x}, \boldsymbol{x}') = \exp(\sum_{k=1,\ldots,n} -\theta_k |x_k - x'_k|)$, where the parameters $\theta_1, ..., \theta_n$ are identified by Maximum Likelihood Estimation (MLE). The regression function is chosen constant, $F = [1 \ ... \ 1]^T$ and $M = (1)$.

2.4. Surrogate modeling. Co-kriging. One of the Pareto set refinement strategies, considered in this work, relies on combining information from EM simulations of various fidelities. Here, it is realized using Co-kriging [30]. Co-kriging is an extension of Kriging, which allows blending the low- and high-fidelity EM simulation data into one surrogate by exploiting correlations between the models of various fidelities [29].

Generation of a Co-kriging model is carried out through sequential construction of the two Kriging models: the first model $\boldsymbol{R}_{s.KRc}$ composed from the low-fidelity training samples ($X_{B.KRc}$, $\boldsymbol{R}_c(X_{B.KRc})$), and the second $\boldsymbol{R}_{s.KRd}$ model generated on the residuals of the high- and low-fidelity samples ($X_{B.KRf}$, $\boldsymbol{R}_d$), where $\boldsymbol{R}_d = \boldsymbol{R}_f(X_{B.KRf}) - \rho \cdot \boldsymbol{R}_c(X_{B.KRf})$. The parameter ρ is a part of MLE of the second model. In the absence of $\boldsymbol{R}_c(X_{B.KRf})$, they can be approximated by the first model, i.e., as $\boldsymbol{R}_c(X_{B.KRf}) \approx \boldsymbol{R}_{s.KRc}(X_{B.KRf})$. Configuration (the choice of the correlation function, regression function, etc.) of both models can be adjusted separately for the low-fidelity data $\boldsymbol{R}_c$ and the residuals $\boldsymbol{R}_d$, respectively. Moreover, both models use the exponential correlation function together with constant regression function $F = [1 \ 1 \ \ldots \ 1]^T$ and $M = (1)$.

The final Co-kriging model $\boldsymbol{R}_{s.CO}(\boldsymbol{x})$ is defined similarly as in (1), i.e.,

$$\boldsymbol{R}_{s.CO}(\boldsymbol{x}) = M\alpha + r(\boldsymbol{x}) \cdot \Psi^{-1} \cdot (\boldsymbol{R}_d - F\alpha) \quad (2)$$

where the block matrices M, F, $r(x)$ and Ψ of (6) can be written as a function of the two underlying Kriging models $R_{s.KRc}$ and $R_{s.KRd}$:

$$r(\boldsymbol{x}) = [\rho \cdot \sigma_c^2 \cdot r_c(\boldsymbol{x}), \rho^2 \cdot \sigma_c^2 \cdot r_c(\boldsymbol{x}, X_{B.KR_f}) + \sigma_d^2 \cdot r_d(\boldsymbol{x})],$$
$$\Psi = \begin{bmatrix} \sigma_c^2 \Psi_c & \rho \cdot \sigma_c^2 \cdot \Psi_c(X_{B.KR_c}, X_{B.KR_f}) \\ 0 & \rho^2 \cdot \sigma_c^2 \cdot \Psi_c(X_{B.KR_f}, X_{B.KR_f}) + \sigma_d^2 \cdot \Psi_d \end{bmatrix}, \quad (3)$$
$$F = \begin{bmatrix} F_c & 0 \\ \rho \cdot F_d & F_d \end{bmatrix}, \qquad M = [\rho \cdot M_c \;\; M_d],$$

where (F_c, σ_c, Ψ_c, M_c) and (F_d, σ_d, Ψ_d, M_d) of (3) are matrices obtained from the $\boldsymbol{R}_{s.KRc}$ and $\boldsymbol{R}_{s.KRd}$, respectively. Generally, σ_c^2 and σ_d^2 are process variances, while $\Psi_c(\cdot, \cdot)$ and $\Psi_d(\cdot,\cdot)$ stand for correlation matrices of two datasets with the optimized θ_k parameters and correlation function of $\boldsymbol{R}_{s.KRc}$ and $\boldsymbol{R}_{s.KRd}$, respectively.

Figure 1 shows the operation of the Co-kriging model using a simple analytical function example. Densely sampled low-fidelity model data supplemented with a few samples of the high-fidelity model allows achieving very good accuracy when the two types of data are blended together (Co-kriging), whereas the accuracy of the Kriging interpolation model solely based on the high-fidelity data is quite limited.

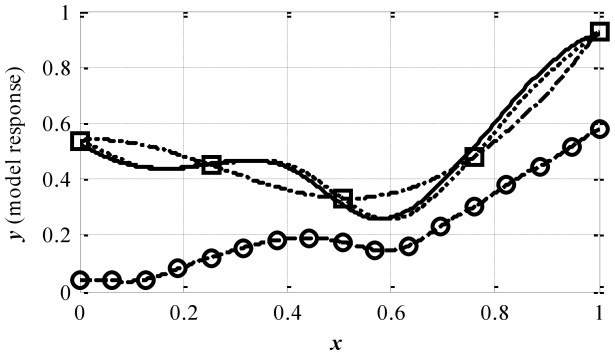

Fig. 1. Co-kriging modeling concept [25]: high-fidelity model (—), low-fidelity model (- - -), high-fidelity model samples (□), low-fidelity model samples (○). Kriging interpolation of the high-fidelity model samples (- · -) is not an adequate representation of the high-fidelity model (due to the limited data set size). Co-kriging interpolation (· · · ·) of blended low- and high-fidelity model data provides much better accuracy at low computational cost

2.5. Optimization algorithm: obtaining initial Pareto set. The initial approximation of the Pareto set is obtained by multi-objective optimization of the fast surrogate model constructed using Kriging interpolation (cf. Subsec. 2.2) and based on sampled low-fidelity EM model data. The design of experiments approach utilized here is Latin Hypercube Sampling [31]. The Kriging model $\boldsymbol{R}_{s.KR}$ is very fast, smooth, and, consequently, easy to optimize. In some cases it might be necessary to perform initial reduction of the design space, that is, identify the subset of the design space containing the Pareto front (which is normally a small part of the original design space [32]). This step is necessary for highly-dimensional design spaces where, without design space reduction, the number of training samples necessary to ensure sufficient surrogate model accuracy is impractically large. Interested reader is referred to [32–34] for exposition of simple design space reduction methods.

Having constructed $\boldsymbol{R}_{s.KR}$, we apply a multi-objective evolutionary algorithm (MOEA) to find a set of designs representing Pareto-optimal solutions with respect to the objectives F_k of interest. Here, we use a standard multi-objective evolutionary algorithm with fitness sharing, Pareto-dominance tournament selection, and mating restrictions [27].

The design optimization flow leading to identification of the initial Pareto set representation is the following:

1. (Optional) Perform design space reduction
2. Sample the design space and acquire the $\boldsymbol{R}_c$ data;
3. Construct the Kriging interpolation model $\boldsymbol{R}_{s.KR}$;
4. (Optional) Correct the Kriging model $\boldsymbol{R}_{s.KR}$ using space mapping;
5. Obtain the Pareto front by optimizing $\boldsymbol{R}_{s.KR}$ using MOEA;

Note that the high-fidelity model $\boldsymbol{R}_f$ is not evaluated in the above procedure. The two method of refining the initial Pareto set so that it can be elevated to the high-fidelity model level are described in Subsecs. 2.6 and 2.7. Step 3 can be executed in case of considerable discrepancy between $\boldsymbol{R}_{s.KR}$ and $\boldsymbol{R}_f$. In that case, before finding the Pareto set, the Kriging model is enhanced by aligning it with the high-fidelity model at certain (usually small) number of designs using space mapping. Typically, output space mapping and frequency scaling are preferred [35].

2.6. Pareto set refinement using response correction. The first refinement approach relies on point-by-point construction of the high-fidelity model Pareto set representation, starting from the designs sampled on the initial Pareto set obtained using the algorithm of Subsec. 2.5. The latter consists of the Pareto optimal solutions of the surrogate, which, because of the discrepancies between $\boldsymbol{R}c$ and $\boldsymbol{R}f$, have to be corrected to adequately represent the high-fidelity model.

Let $\boldsymbol{x}_s^{(k)}$, $k = 1, \ldots, K$, be the selected elements of the Pareto front found by the MOEA. For simplicity of the notation, the design refinement stage below is defined assuming two objectives F_1 and F_2; however, it can be generalized for any value of N_{obj}. The refinement stage exploits the output space mapping (OSM) [35] process of the following form:

$$\boldsymbol{x}_f^{(k.i+1)} = \arg \min_{\boldsymbol{x},\, F_2(\boldsymbol{x}) \le F_2(\boldsymbol{x}_s^{(k.i)})} F_1 \cdot \left(\boldsymbol{R}_s(\boldsymbol{x}) + [\boldsymbol{R}_f(\boldsymbol{x}_s^{(k.i)}) - \boldsymbol{R}_s(\boldsymbol{x}_s^{(k.i)})] \right). \quad (4)$$

The optimization process (4) is constrained not to increase the second objective as compared to $\boldsymbol{x}_s^{(k)}$. The surrogate model $\boldsymbol{R}_s$ is corrected using the OSM term $\boldsymbol{R}_f(\boldsymbol{x}_s^{(k.i)}) - \boldsymbol{R}_s(\boldsymbol{x}_s^{(k.i)})$ (here, $\boldsymbol{x}_f^{(k.0)} = \boldsymbol{x}_s^{(k)}$), so that the corrected surrogate model coincides with $\boldsymbol{R}_f$ at the beginning of each iteration. In practice, two or three iterations of (4) are sufficient to find a refined high-fidelity model design $\boldsymbol{x}_f^{(k)}$. After completing this stage, we create a set of Pareto-optimal high-

fidelity model designs. This set is the final outcome of our multi-objective optimization process.

2.7. Pareto set refinement using Co-kriging surrogates. An alternative approach to Pareto set refinement is by using Co-kriging surrogates (cf. Subsec. 2.4). In this case, the high-fidelity model evaluated at the designs sampled from the initial Pareto set obtained by optimizing $\boldsymbol{R}_{s.KR}$ are included into the surrogate model so that it becomes more and more accurate representation of $\boldsymbol{R}_f$ at least in the vicinity of the Pareto front.

The design algorithm flow is as follows:

1. Evaluate high-fidelity model $\boldsymbol{R}_f$ at selected locations along the current Pareto front representation;
2. Update the Co-kriging surrogate $\boldsymbol{R}_{s.CO}$ (cf. (2));
3. Update Pareto set by optimizing $\boldsymbol{R}_{s.CO}$ using MOEA;
4. If termination condition is not satisfied go to 2; else END

When executing Step 1 for the first time, the current Pareto front representation is a Pareto set obtained using the algorithm of Subsec. 2.5. Typically, about 10 high-fidelity model evaluations are used in Step 1, and the number of iterations necessary to converge is two to three. Our convergence criterion is the maximum distance between the Pareto front estimated in 3 and the sampled $\boldsymbol{R}_f$ data (here, we use 0.5 dB for reflection objective). It should be emphasized that – upon convergence – the entire Pareto set generated by the above procedure (not just a set of design sampled from it) is a reliable representation of the high-fidelity Pareto set.

3. Case study 1: UWB monocone

In this section we demonstrate the multi-objective optimization procedure exploiting both Pareto front refinement schemes described in Subsecs. 2.6 and 2.7, respectively. The methods are illustrated using an ultra-wideband (UWB) antenna in the form of a monocone. The design objectives are footprint reduction and minimization of reflection.

3.1. UWB monocone – antenna description. Consider a monocone structure [24] that operates in the UWB frequency band. The antenna is fed directly through 50-Ohm coaxial line with Teflon filling and outer diameter of 0.635 mm. A parameter vector: $\boldsymbol{x} = [z_1\ z_2\ r_1]^T$ represents antenna design variables. All parameter values are expressed in mm. The antenna geometry is shown in Fig. 2.

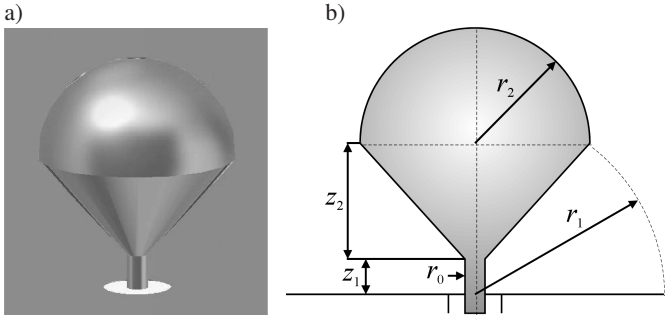

Fig. 2. UWB monocone: a) 3D view; b) the cut view, after Ref. 24

Two computational models of the antenna are implemented in CST Microwave Studio and evaluated using its transient solver [7]. The high-fidelity model $\boldsymbol{R}_f$ is consists of about 1,400,000 hexahedral mesh cells and its average evaluation time is 23 min, whereas its less accurate counterpart $\boldsymbol{R}_c$ is generated using 33,000 hexahedral mesh cells. An average simulation time of the latter is 33 s and it is 42 times faster than $\boldsymbol{R}_f$.

In this example, we consider two design objectives: (i) minimization of antenna reflection within UWB (3.1 GHz to 10.6 GHz) frequency band (objective F_1), and (ii) reduction of antenna footprint (objective F_2), which is defined as a maximum dimension out of vertical and lateral ones: $S = \max\{2r_2, z_1+z_2+r_2\}$. The symbol $r_2 = (r_1^2-(z_1+z_2)^2)^{1/2}$ denotes the radius of the hemisphere terminating the monopole.

3.2. UWB monocone. Generation of initial Pareto set. The solution space for multi-objective antenna optimization is defined by the lower and upper bounds $\boldsymbol{l} = [0\ 2\ 4]^T$ and $\boldsymbol{u} = [4\ 15\ 20]^T$. A Kriging surrogate model constructed using 600 low-fidelity model samples is optimized using methodology of Subsec. 2.5. The initial Pareto optimal set is shown in Fig. 3a, whereas visualization of Pareto optimal design variables within a defined solution space is illustrated in Fig. 3b.

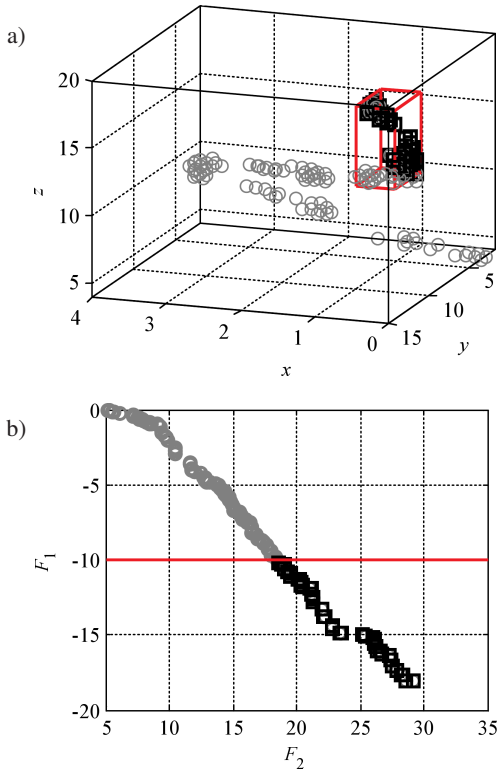

Fig. 3. UWB monocone antenna: a) visualization of the Pareto optimal set (○) in 3-dimensional solution space. The portion of the design space that contains the part of the Pareto set we are interested in (red cuboid, where $F_1 \leq -10$), b) the part of the Pareto set that is of interest from the point of view of adequate antenna operation (□) versus the entire one mapped to the feature space (○)

One should note that despite the Pareto set range for objective F_1 being from below – 20 up to near 0 dB, the antenna is considered as operating properly if it can provide in-band reflection below the level of -10 dB or lower. Therefore, only the designs that fulfill this requirement are considered relevant, and they are the subject of Pareto set refinement (cf. Subsec. 3.3 and Subsec. 3.4).

3.3. UWB monocone. Pareto set refinement using response correction. A set of 10 designs selected from the initial Pareto set have been refined using the response correction technique of Subsec. 2.6 in order to obtain high-fidelity representation of the Pareto front. Two refinement steps (per design) were required to obtain the final solutions. The geometrical details of the refined solutions are listed in Table 1. A comparison of a Pareto front obtained through $\boldsymbol{R}_s$ model optimization and its representation based on a set of 10 refined $\boldsymbol{R}_f$ model samples is shown in Fig. 4.

Table 1
Refined designs of the optimized UWB monocone antenna

F_1	F_2	Design Variables [mm]		
		z_1	z_2	r_1
−9.5	18	0.994	10.36	13.16
−10.9	19	0.021	12.18	12.97
−11.6	20	0.065	12.48	14.59
−12.3	21	0.051	12.84	15.23
−13.2	22	0.000	12.92	15.79
−14.7	23	0.000	12.06	16.28
−16.0	24	0.008	12.08	16.97
−17.1	25	0.079	12.42	17.68
−18.1	26	0.142	12.99	18.38
−18.4	27	0.169	13.43	19.09
−19.4	28	0.231	13.27	19.45

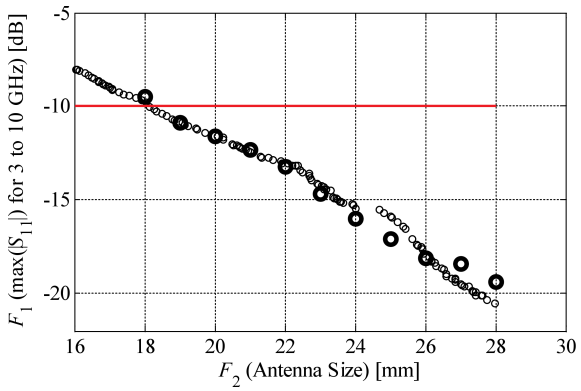

Fig. 4. Comparison of the Pareto front obtained from optimized $\boldsymbol{R}_s$ model (○) and eleven (see Table 1) refined $\boldsymbol{R}_f$ model designs (□)

The smallest footprint of an antenna that still satisfies the minimum requirements upon its reflection (objective F_2) is 19 mm, whereas the lowest in-band reflection (objective F_1) is -19.4 dB. Variations of objectives for extreme designs are 32% and 44% for the former and the latter, respectively.

The total cost of design optimization corresponds to only 44 $\boldsymbol{R}_f$ model evaluations (about 17 hours of CPU time) and it includes: 600 $\boldsymbol{R}_c$ simulations ($\sim$14 $\boldsymbol{R}_f$ evaluations) for design of experiment (cf. Subsec. 3.2), and 10 $\boldsymbol{R}_f$ for initial evaluation and refinement (2×10 $\boldsymbol{R}_f$) of selected samples. The computational cost of MOEA optimization (a few dozen thousands of $\boldsymbol{R}_s$ model evaluations) is negligible in comparison with the cost of antenna models simulation, thus it is not included here.

3.4. UWB monocone. Pareto set refinement using co-kriging. A set of 10 design samples is chosen from the initial Pareto set (cf. Subsec. 2.5) and evaluated to obtain their high-fidelity model responses. Subsequently a Co-kriging methodology of Subsec. 2.7 is utilized to refine the Pareto set. The final Pareto set representation was obtained in three iterations of the algorithm (cf. Subsec. 2.7). It should be noted that high-fidelity model samples gathered across iterations are incorporated into the Co-kriging model to increase its accuracy. A comparison of initial and refined Pareto set as well as 10 responses of evenly chosen high-fidelity model designs evaluated for verification purpose is shown in Fig. 5. The dimensions of selected antennas are shown in Table 2. The minimum antenna footprint that satisfies requirements upon reflection (objective F_1) is 32% smaller in comparison to the structure with the best in-band reflection (objective F_2) of -19.4 dB.

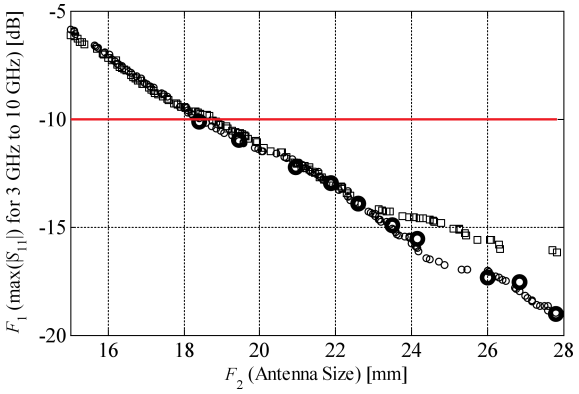

Fig. 5. UWB monocone antenna: initial Pareto set approximation (○), final Pareto set obtained after three iterations of the proposed methodology (□), selected high-fidelity model designs (□) evaluated for verification purpose

Table 2
Selected designs of the optimized UWB monocone antenna

F_1	F_2	Design Variables [mm]		
		z_1	z_2	r_1
−10.1	18	0.23	11.79	13.61
−10.6	19	0.18	11.80	13.81
−11.1	20	0.28	11.63	14.44
−12.2	21	0.06	12.22	15.03
−13.6	22	0.06	11.76	15.81
−14.9	23	0.06	12.62	16.67
−16.5	24	0.05	12.66	17.31
−17.3	26	0.17	13.39	18.41
−17.6	27	0.21	13.38	18.98
−19.0	28	0.25	13.55	19.59

The total aggregated cost of the design optimization process corresponds to about 44 evaluations of the high-fidelity model, i.e., ∼17 hours of CPU time (including 600 × $\boldsymbol{R}_c \approx 14 \times \boldsymbol{R}_f$ for initial Kriging model construction, and 3 × 10 × $\boldsymbol{R}_f = 30 \times \boldsymbol{R}_f$ for three iterations of the surrogate enhancement). The computational cost of MOEA optimization of the Co-kriging model is not included for the same reasons as mentioned in Subsec. 3.4.

4. Case study 2. Planar Yagi-Uda antenna

Our second example is a planar Yagi-Uda antenna with a single director. Similarly as for the previous example, we demonstrate the use of the two design refinement strategies. Here, the objectives of interest are the average gain and in-band reflection.

4.1. Planar Yagi-Uda. Antenna description. Consider a planar Yagi-Uda antenna [36] shown in Fig. 6. It is composed of a driven element fed by a microstrip-to-cps transition, a director, and a balun. The input impedance is 50-Ohm and the structure is designated to operate on a Rogers RT6010 dielectric substrate ($\varepsilon_r = 10.2$, tan$\delta = 0.0023$, $h = 0.635$ mm). A structure is described by a eight adjustable parameters: $\boldsymbol{x} = [s_1\ s_2\ v_1\ v_2\ u_1\ u_2\ u_3\ u_4]^T$. Additional parameters, i.e., Parameters $w_1 = 0.6$, $w_2 = 1.2$, $w_3 = 0.3$ and $w_4 = 0.3$ remain fixed. All dimensions are expressed in mm. The design space is defined by the lower and upper bounds $\boldsymbol{l} = [3.8\ 2.8\ 8.0\ 4.0\ 3.0\ 4.5\ 1.8\ 1.3]^T$ and $\boldsymbol{u} = [4.4\ 4.4\ 9.8\ 5.2\ 4.2\ 5.2\ 2.6\ 1.8]^T$.

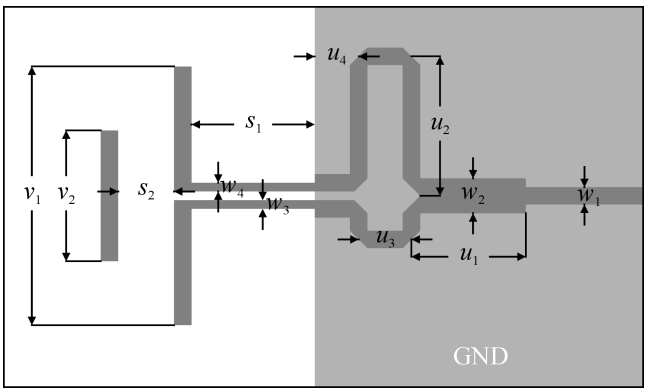

Fig. 6. Geometry of a planar Yagi-Uda antenna

Both the high-fidelity model $\boldsymbol{R}_f$ composed of about 1,400,000 hexahedral mesh cells (average simulation time of 36 min) and the low-fidelity model $\boldsymbol{R}_c$ containing about 100,000 mesh cells are implemented in CST Microwave Studio (average simulation time 90 s). It should be noted that $\boldsymbol{R}_c$ is 24 times faster than $\boldsymbol{R}_f$.

There are two design objectives: (i) minimization of antenna in-band reflection (objective F_1) and (ii) maximization of average gain (objective F_2), both within 10 to 11 GHz bandwidth.

4.2. Planar Yagi-Uda antenna. Design with response correction. Direct multi-objective optimization of discussed planar Yagi-Uda structure is not possible due to a very large number of low-fidelity model samples required for the generation of $\boldsymbol{R}_s$ model in the original design space. For that reason, the procedure of Subsec. 2.5 cannot be directly applied for the considered antenna. This difficulty has been alleviated by decomposing the structure into two complementary sub-circuits, i.e., the radiator and a balun (see Fig. 7), which allows reducing the number of independent design variables that participate in $\boldsymbol{R}_s$ model generation to four for each antenna sub-structure. Subsequently, design of experiments is conducted in corresponding sub-spaces and the antenna surrogate model $\boldsymbol{R}_s$ is recomposed using circuit theory rules. Such decomposition is feasible in this case because the balun is primarily responsible for the reflection response of the antenna but not for its radiation properties. A detailed description of the decomposition procedure is omitted for the sake of brevity. A more detailed explanation is provided in [24].

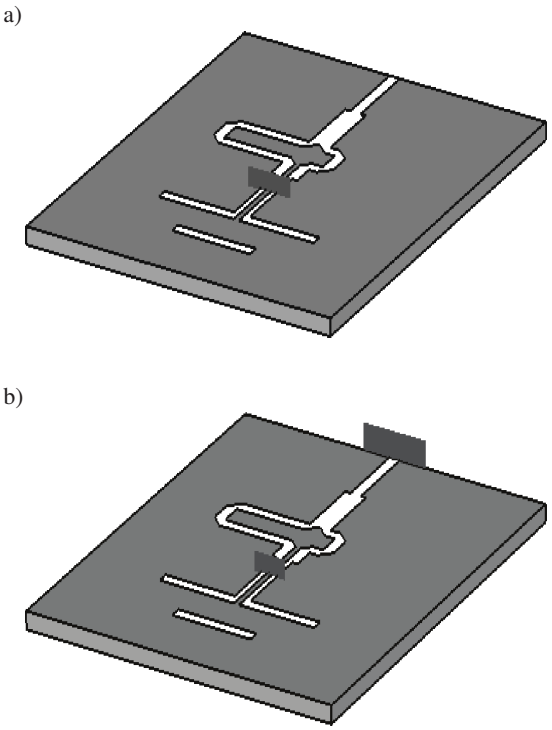

Fig. 7. Visualization of a decomposition procedure, low-fidelity model of: (a) a radiator with excitation applied directly to the coplanar slot-line; (b) a balun with two ports ([24]); the balun and the radiator are physically present in (a) and (b) to account for EM couplings between subcircuits

The surrogate model $\boldsymbol{R}_s$ of the Yagi-Uda antenna is optimized using MOEA and solutions with $F_1 \leq -10$ dB are utilized in the refinement procedure (cf. Subsec. 3.3). Subsequently, response correction technique of Subsec. 2.6 is carried out to refine nine designs evenly distributed along the initial Pareto set. The final solutions are obtained after two iterations of refinement procedure each. A comparison of the initial Pareto set based on $\boldsymbol{R}_s$ model evaluations and its repre-

sentation composed of $\boldsymbol{R}_f$ model responses is shown in Fig. 8, whereas the geometrical details are listed in Table 3. The average gain and reflection varies over the Pareto front from 5.6 dB to 6.4 dB (13%) and from −18.3 dB up to −10 dB (45%), respectively.

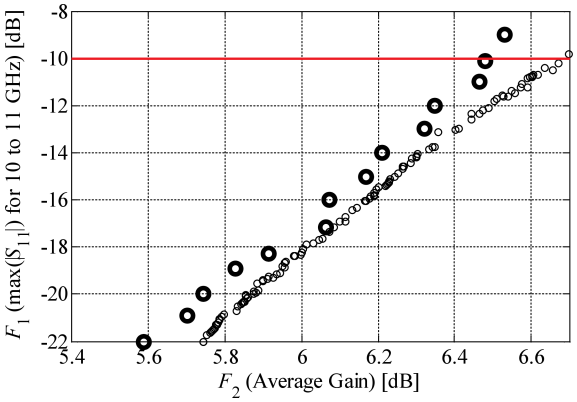

Fig. 8. Comparison of the Pareto front obtained from optimized $\boldsymbol{R}_s$ model (○) and refined 14 $\boldsymbol{R}_f$ model designs (□)

Table 3
Refined designs of the optimized planar Yagi-Uda antenna

F_1	F_2	Design Variables [mm]							
		s_1	s_2	v_1	v_2	u_1	u_2	u_3	u_4
−10.1	6.5	4.34	4.25	8.26	5.12	3.92	4.75	2.20	1.65
−12.0	6.3	4.36	4.22	8.46	5.03	3.85	4.86	2.20	1.63
−14.0	6.2	4.31	4.26	8.57	4.87	3.90	4.82	2.17	1.64
−16.0	6.1	4.30	4.25	8.76	4.77	3.88	4.84	2.21	1.65
−18.3	5.9	4.33	4.21	8.77	4.65	3.81	4.86	2.16	1.62
−20.0	5.7	4.22	3.82	9.13	4.68	3.87	4.83	2.22	1.68
−22.0	5.6	4.15	3.55	9.29	4.68	3.87	4.80	2.21	1.73
−24.0	5.5	4.16	3.38	9.34	4.67	3.90	4.76	2.20	1.72
−24.8	5.2	4.13	3.23	9.55	4.65	3.92	4.72	2.19	1.68

The total cost of design optimization is about 77 $\boldsymbol{R}_f$ model evaluations (∼29 hours). It includes: acquisition of the low-fidelity simulation data for Kriging model construction (total cost corresponds to about 60 $\boldsymbol{R}_f$ model evaluations), and a total of 27 $\boldsymbol{R}_f$ model evaluations for high fidelity model evaluation and refinement. Similarly to previous cases, the cost of MOEA optimization is neglected.

4.3. Planar Yagi-Uda antenna. Pareto set refinement using Co-kriging. As indicated in Fig. 2, the Pareto set normally occupies a very small fraction of the original design space. Here, in order to allow construction of the initial Kriging surrogate model using reasonably small number of samples (not possible in the original design space), we perform reduction of the design space through finding two extreme points of the Pareto set by means of single-objective optimizations with respect to each considered objectives, one at a time. The reduced space is determined by the following lower and upper frontiers: $\boldsymbol{l} = [4.1\ 3.3\ 8.3\ 4.6\ 3.8\ 4.7\ 2.1\ 1.5]^T$ and $\boldsymbol{u} = [4.4\ 4.3\ 9.3\ 5.2\ 4.0\ 4.9\ 2.3\ 1.8]^T$. For the sake of brevity we omit details related to design space reduction techniques. Interested reader is referred to the literature (e.g., [32–34]). The Kriging surrogate model is constructed using a set of 500 samples (cf. Subsec. 2.5) and optimized using MOEA. Only the solutions with $F_1 \leq -10$ dB are considered as relevant for the refinement (cf. Subsec. 3.3).

The initial Pareto front utilized for the refinement is obtained using MOEA of $\boldsymbol{R}_s$ model constructed within reduced solution space. The designs are refined using co-Kriging technique (cf. Subsec. 2.5). Only two iterations of the algorithm were needed to obtain the final Pareto front. A comparison of initial and refined sets is illustrated in Fig. 9. Detailed dimensions of a 10 selected antenna designs are collected in Table 4. The maximum antenna gain (6.5 dB) comes with the lowest obtained reflection (−10.6 dB) and if varies by 15% along the Pareto optimal set. Moreover, the lowest reflection value is −18 dB (corresponding gain is 5.5 dB).

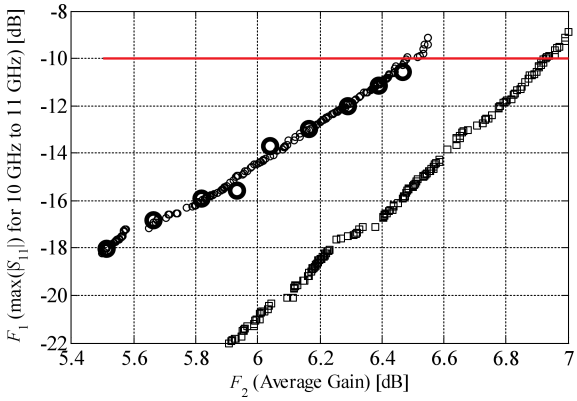

Fig. 9. Initial Pareto set approximation (○), final Pareto set obtained after three iterations of the proposed methodology (□) and 9 selected high-fidelity model designs (□) of a planar Yagi-Uda antenna

Table 4
Selected designs of the optimized planar Yagi-Uda antenna

F_1	F_2	Design Variables [mm]							
		s_1	s_2	v_1	v_2	u_1	u_2	u_3	u_4
−10.6	6.5	4.27	4.26	8.34	5.12	3.87	4.77	2.19	1.72
−11.2	6.4	4.27	4.26	8.32	5.05	3.85	4.83	2.17	1.72
−12.0	6.3	4.25	4.27	8.33	4.93	3.85	4.83	2.17	1.72
−13.0	6.2	4.30	4.19	8.33	4.83	3.89	4.80	2.16	1.73
−13.5	6.0	4.30	4.05	8.38	4.78	3.92	4.76	2.19	1.64
−15.7	5.9	4.21	4.07	8.63	4.66	3.85	4.85	2.14	1.61
−15.9	5.8	4.23	3.83	8.64	4.67	3.84	4.84	2.14	1.62
−16.8	5.7	4.23	3.57	8.77	4.67	3.86	4.82	2.15	1.62
−18.0	5.5	4.14	3.33	9.20	4.73	3.84	4.82	2.23	1.58

The total aggregated cost of the design optimization process corresponds to ∼39 $\boldsymbol{R}_f$ model simulations (∼23 hours). The cost includes: 500× $\boldsymbol{R}_c \approx 21\times \boldsymbol{R}_f$ for a construction of initial Kriging model and 18 × $\boldsymbol{R}_f$ for two iterations of the Co-kriging algorithm. The cost of MOEA optimization is excluded.

5. Discussion and conclusions

In this paper, we have reviewed two recent techniques for computationally efficient multi-objective design of antennas.

The presented methods utilize an evolutionary algorithm and fast surrogate models constructed using Kriging interpolation of low-fidelity simulation data. Two alternative techniques for refinement of the Pareto optimal set, i.e., response correction, and Co-kriging, are discussed. The methods are illustrated using two exemplary antennas, a three-variable UWB monocone structure and an eight-variable planar Yagi-Uda antenna. Both techniques allow for generating the Pareto front representation at a cost corresponding to several dozens of high-fidelity model evaluations, which is only a small fraction of the cost required by direct multi-objective optimization of EM antenna models using population-based MOEA, the latter usually being well over several thousands of objective evaluations.

It should also be noted that several techniques for handling the design space for the purpose of surrogate model construction have been utilized, including: preparation of surrogate model within the original solution space (sufficient for lower-dimensional case), decomposition of the antenna structure into sub-circuits and construction of surrogate models in corresponding subspaces, as well as design space reduction. Slight differences between the Pareto sets obtained during the numerical tests are partially due to utilizing these various approaches.

Although both Pareto set refinement methods generate similar results, the response correction technique is significantly simpler to implement than Co-kriging. The method utilizes output space mapping for a point-by-point refinement of representative antenna designs selected along the Pareto set. The latter approach requires iterative construction and re-optimization of a surrogate model that incorporates both high- and low-fidelity model samples. On the other hand, Co-kriging allows for obtaining more complete Pareto set, not just a few selected designs along it. Also, for the response correction technique, the cost of generating the Pareto set representation increases with the number of required final designs, whereas it is essentially constant for the Co-kriging-based method.

The methods discussed in this paper are promising for rapid multi-objective optimization of expensive EM-simulation-based antenna models. However, there are some issues that should be addressed by the future research. Perhaps the most important one is design space confinement aimed at identifying the design space region that contains Pareto optimal designs. This is particularly important for handling problems with larger number of variables ($>$10–15). On the other hand, for certain types of structures (e.g., narrow-band antennas) it might be necessary to apply low-fidelity model correction before attempting to construct the response surface approximation surrogate, which because of the original misalignment between EM simulation models of different fidelities may be too large to be accommodated at the design refinement stage. Addressing the aforementioned issues may results in increasing the range of application of the presented techniques.

Acknowledgements. The authors would like to thank the Computer Simulation Technology AG, Darmstadt, Germany, for making CST Microwave Studio available. This work was supported in part by the Icelandic Centre for Research (RANNIS), the Grant 130450051, and by the National Science Centre of Poland, the Grants 2013/11/B/ST7/04325 and 2014/12/ST7/00045.

REFERENCES

[1] H. Schantz, *The Art and Science of Ultrawideband Antennas*, Artech House, London, 2005.

[2] J. Volakis, C.-C. Chen, and K. Fujimoto, *Small Antennas: Miniaturization Techniques and Applications,* McGraw-Hill Professional, London, 2010.

[3] F.B. Gross, *Frontiers in Antennas: Next Generation Design & Engineering*, McGraw-Hill Professional, London, 2011.

[4] S. Koziel, F. Mosler, S. Reitzinger, and P. Thoma, "Robust microwave design optimization using adjoint sensitivity and trust regions", *Int. J. RF and Microwave CAE* 22, 10–19 (2012).

[5] D. Nair and J.P. Webb, "Optimization of microwave devices using 3-D finite elements and the design sensitivity of the frequency response", *IEEE Trans. Magn.* 39, 1325–1328 (2003).

[6] J.I. Toivanen, J. Rahola, R.A.E. Makinen, S. Jarvenpaa, and P. Yla-Oijala, "Gradient-based antenna shape optimization using spline curves", *Ann. Review Progress in Applied Comp. Electromagnetics* 1, 908–913 (2010).

[7] *CST Microwave Studio,* ver. 2012, CST AG, Bad Nauheimer Str. 19, D-64289 Darmstadt, 2012.

[8] *Ansys HFSS*, ver. 14.0 (2012), ANSYS, Inc., Southpointe 275 Technology Drive, Canonsburg, PA 15317.

[9] J.W. Bandler, Q.S. Cheng, S.A. Dakroury, A.S. Mohamed, M.H. Bakr, K. Madsen, and J. Søndergaard, "Space mapping: the state of the art", *IEEE Trans. Microwave Theory Tech.* 52, 337–361 (2004).

[10] S. Koziel, S. Ogurtsov, and S. Szczepanski, "Rapid antenna design optimization using shape-preserving response prediction", *Bull. Pol. Ac.: Tech.* 60 (1), 143–149 (2012).

[11] S. Koziel and S. Ogurtsov, "Rapid design optimization of antennas using space mapping and response surface approximation models", *Int. J. RF & Microwave CAE* 21, 611–621 (2011).

[12] I. Couckuyt, S. Koziel, and T. Dhaene, "Surrogate modeling of microwave structures using kriging, co-kriging and space mapping", *Int. J. Numerical Modelling: Electronic Devices and Fields* 26, 64–73 (2013).

[13] S. Koziel and J.W. Bandler, "Accurate modeling of microwave devices using kriging-corrected space mapping surrogates", *Int. J. Numerical Modelling* 25, 1–14 (2012).

[14] S. Koziel and S. Ogurtsov, "Model management for cost-efficient surrogate-based optimization of antennas using variable-fidelity electromagnetic simulations", *IET Microwaves Ant. Prop.* 6, 1643–1650 (2012).

[15] S. Koziel and S. Ogurtsov, *Antenna Design by Simulation-Driven Optimization*, Springer, Berlin, 2014.

[16] S. Koulouridis, D. Psychoudakis, and J. Volakis, "Multiobjective optimal antenna design based on volumetric material optimization", *IEEE Tran. Antennas Propag.* 55, 594–603 (2007).

[17] Y. Kuwahara, "Multiobjective optimization design of Yagi–Uda antenna", *IEEE Tran. Antennas Propag.* 53, 1984–1992 (2005).

[18] M. John and M.J. Ammann, "Antenna optimization with a computationally efficient multiobjective evolutionary algorithm", *IEEE Tran. Antennas Propag.* 57, 260–263 (2007).

[19] T. Maruyama, K. Yamamori, and Y. Kuwahara, "Design of multibeam dielectric lens antennas by multiobjective optimization", *IEEE Tran. Antennas Propag.* 57, 57–63 (2007).

[20] N. Jin and Y. Rahmat-Samii, "Advances in particle swarm optimization for antenna designs: real-number, binary, single-objective and multiobjective implementations", *IEEE Tran. Antennas Propag.* 55, 556–567 (2007).

[21] B. Aljibouri, E.G. Lim, H. Evans, and A. Sambell, "Multi-objective genetic algorithm approach for a dual-feed circular polarised patch antenna design", *Electronic Letters* 36, 1005–1006 (2000).

[22] S. Chamaani, M.S. Abrishamian, and S.A. Mirtaheri, "Time-domain design of UWB Vivaldi antenna array using multi-objective particle swarm optimization", *IEEE Antennas and Wireless Prop. Lett.* 9, 666–669 (2010).

[23] H. Choo, R.L. Rogers, and H. Ling, "Design of electrically small wire antennas using a pareto genetic algorithm", *IEEE Trans. Antennas Prop.* 53, 1038–1046 (2005).

[24] S. Koziel and S. Ogurtsov, "Multi-objective design of antennas using variable-fidelity simulations and surrogate models", *IEEE Trans. Antennas Prop.* 61, 5931–5939 (2013).

[25] S. Koziel, A. Bekasiewicz, I. Couckuyt, and T. Dhaene, "Efficient multi-objective simulation-driven antenna design using Co-kriging", *IEEE Tran. Antennas Propag.* 62, 5900–5905 (2014).

[26] M.C. Kennedy and A. O'Hagan, "Predicting the output from complex computer code when fast approximations are available", *Biometrika* 87, 1–13 (2000).

[27] K. Deb, *Multi-Objective Optimization Using Evolutionary Algorithms*, John Wiley & Sons, New York, 2001.

[28] S. Koziel, and S. Ogurtsov, "Model management for cost-efficient surrogate-based optimization of antennas using variable-fidelity electromagnetic simulations", *IET Microwaves Antennas Prop.* 6, 1643–1650 (2012).

[29] T.W. Simpson, J. Peplinski, P.N. Koch, and J.K. Allen, "Metamodels for computer-based engineering design: survey and recommendations", *Engineering with Computers* 17, 129–150 (2001).

[30] A.I. Forrester, A. Sobester, and A.J. Keane, "Multi-fidelity optimization via surrogate modelling", *Proc. Royal Society* 463, 3251–3269 (2007).

[31] B. Beachkofski and R. Grandhi, "Improved distributed hypercube sampling", *American Institute of Aeronautics and Astronautics* AIAA 2002, 1274 (2002).

[32] A. Bekasiewicz, S. Koziel, and W. Zieniutycz, "Design space reduction for expedited multi-objective design optimization of antennas in highly-dimensional spaces", in *Solving Computationally Extensive Engineering Problems: Methods and Applications*, Springer, Berlin, 2014.

[33] S. Koziel, A. Bekasiewicz, and W. Zieniutycz, "Expedite EM-driven multi-objective antenna design in highly-dimensional parameter spaces", *IEEE Antennas and Wireless Propagation Letters* 13, 631–634 (2014).

[34] A. Bekasiewicz, S. Koziel, and L. Leifsson, "Low-cost EM-simulation-driven multi-objective optimization of antennas", *Int. Conf. Computational Science*, in *Procedia Computer Science* 29, 790–799 (2014).

[35] S. Koziel, Q.S. Cheng, and J.W. Bandler, "Space mapping", *IEEE Microwave Magazine* 9, 105–122 (2008).

[36] Y. Qian, W.R. Deal, N. Kaneda, and T. Itoh, "Microstrip-fed quasi-Yagi antenna with broadband characteristics", *Electronics Letters* 34, 2194-2196 (1998).

[37] J. Kwiecien and B. Filipowicz, "Comparison of firefly and cockroach algorithms in selected discrete and combinatorial problems", *Bull. Pol. Ac.: Tech.* 62 (4), 797–804 (2014).

[38] T. Lewinski, S. Czarnecki, G. Dzierzanowski, and T. Sokol, "Topology optimization in structural mechanics", *Bull. Pol. Ac.: Tech.* 61 (1), 23–37 (2013).

[39] B. Blachowski and W. Gutkowski, "Graph based discrete optimization in structural dynamics", *Bull. Pol. Ac.: Tech.* 62 (1), 91–102 (2014).